

*Citation for published version:*

Tiong, TJ, Price, GJ & Kanagasisingam, S 2014, 'A computational simulation study on the acoustic pressure generated by a dental endosonic file: effects of intensity, file shape and volume', *Ultrasonics Sonochemistry*, vol. 21, no. 5, pp. 1858-1865. <https://doi.org/10.1016/j.ultsonch.2014.03.024>

*DOI:*

[10.1016/j.ultsonch.2014.03.024](https://doi.org/10.1016/j.ultsonch.2014.03.024)

*Publication date:*

2014

*Document Version*

Peer reviewed version

[Link to publication](#)

*Publisher Rights*

Unspecified

**University of Bath**

**Alternative formats**

If you require this document in an alternative format, please contact:  
[openaccess@bath.ac.uk](mailto:openaccess@bath.ac.uk)

**General rights**

Copyright and moral rights for the publications made accessible in the public portal are retained by the authors and/or other copyright owners and it is a condition of accessing publications that users recognise and abide by the legal requirements associated with these rights.

**Take down policy**

If you believe that this document breaches copyright please contact us providing details, and we will remove access to the work immediately and investigate your claim.

1     **A COMPUTATIONAL SIMULATION STUDY ON THE ACOUSTIC**  
2     **PRESSURE GENERATED BY A DENTAL ENDOSONIC FILE:**  
3     **EFFECTS OF INTENSITY, FILE SHAPE AND VOLUME**

4             T. Joyce Tiong<sup>a,b\*</sup>, Gareth J. Price<sup>b</sup> and Shalini Kanagasingam<sup>c</sup>

6             <sup>a</sup> Manufacturing and Industrial Processes Research Division, Faculty of Engineering,  
7             University of Nottingham Malaysia campus, 43500 Semenyih, Selangor, Malaysia.

8             <sup>b</sup> Department of Chemistry, University of Bath, Claverton Down, Bath BA2 7AY, United  
9             Kingdom.

10            <sup>c</sup> Department of Dentistry, Universiti Kebangsaan Malaysia, Jalan Raja Muda Abdul Aziz,  
11            50300 Kuala Lumpur, Malaysia.

25     \*Corresponding Author. Tel.: +6 03 8725 3495     Fax: + 6 03 8924 8017  
26     Email address: [joyce.tiong@nottingham.edu.my](mailto:joyce.tiong@nottingham.edu.my)

## Abstract

One of the uses of ultrasound in dentistry is in the field of endodontics (i.e. root canal treatment) in order to enhance cleaning efficiency during the treatment. The acoustic pressures generated by the oscillation of files in narrow channels has been calculated using the COMSOL simulation package. Acoustic pressures in excess of the cavitation threshold can be generated and higher values were found in narrower channels. This parallels experimental observations of sonochemiluminescence. The effect of varying the channel width and length and the dimensions and shape of the file are reported. As well as explaining experimental observations, the work provides a basis for the further development and optimisation of the design of endosonic files.

*Keywords: endodontic, cleaning, acoustic pressure, cavitation, COMSOL.*

## Highlights:

- Acoustic pressure generated is affected by the working volume.
- Endosonic files were able to generate high acoustic pressures in a confined space.
- The acoustic pressure generated contributes to the production of cavitation.
- Decrease in size of the root canal model causes an increase in acoustic pressure.

49 **Nomenclature**

50	SCL	sonochemiluminescence
51	$d$	diameter of the endosonic file, mm
52	$l$	length of the endosonic file, mm
53	$D$	diameter of the root canal model, mm
54	$L$	length of the root canal model, mm
55	$P_{US}$	ultrasonic power, W
56	$I$	ultrasonic intensity, W m <sup>-2</sup>
57	$A$	area, m <sup>2</sup>
58	$R$	radius of the endosonic file, mm
59	$p_o$	acoustic pressure amplitude, Pa
60	$\rho$	density, kg m <sup>-3</sup>
61	$c$	speed of sound, m s <sup>-1</sup>
62	$t$	time, s
63	$P$	acoustic pressure, Pa
64	$r$	spatial variable ( $r = [x,y,z]$ )
65	$\omega$	angular frequency, rad s <sup>-1</sup>
66	$\kappa$	wave number ( $\kappa = \omega/c$ )
67	$h$	stepsize
68	$n$	normal vector
69	$Z$	acoustic impedance, Rayl
70	PMMA	polymethylmethacrylate
71	$x$	distance from ultrasonic source, m
72	$TL$	transmission loss, dB
73	$R_c$	reflective coefficient
74	$T_c$	transmission coefficient

75

## 1. Introduction

Acoustic cavitation is a well-known phenomenon in the field of ultrasound [1]. It can increase mixing and fluid motion in a system, form reactive intermediates which accelerate chemical reactions and aid in cleaning processes [2, 3]. Ultrasound is used in dentistry to aid in cleaning. One of the most common applications of power ultrasound in dentistry is in periodontics where ultrasound with frequencies of 20 – 40 kHz is used in dental scalers to remove dental debris and plaque around the teeth and gums [4]. Apart from the mechanical cleaning effects, recent studies have shown that cavitation can be produced in water around the scalers [5], and the amount of cavitation and its distribution around the instrument has a strong correlation with the shape and design of the tip [6-8].

Another application of ultrasound in dentistry is in endodontics (root canal treatment). Here, ultrasound is applied to a narrow file which is placed within the root canal to improve the dissolution and removal of infected tissues and abscess from an infected root canal [9]. A number of researchers have shown that ultrasonically assisted irrigation improves the cleaning efficiency in root canal treatments [10-12]. Some argued that this was due to enhanced acoustic streaming [13-15] while others suggested that it could be due to the physical effects caused by cavitation [5, 8]. The oscillation profiles of endosonic files (i.e. files used during endodontic treatments that involve ultrasonic vibrations) have been measured to investigate correlations between the oscillation profiles and the cleaning effectiveness [16, 17]. The areas of cavitation activity around the instruments were assessed by the detection of sonochemiluminescence (SCL). Although it was reported that SCL tended to appear around the vibration antinodes of the oscillating files, there was no clear relation between the vibration amplitudes and the SCL emission [5, 6]. Furthermore, it was also

reported that there was no correlation between the lengths of the endosonic files and the oscillation profiles [18].

Macedo and co-workers recently suggested that the production of SCL was greatly increased when an endosonic file was operated in a human-sized root canal model as compared with in a cuvette of 10 mm wide and claimed that it was due to higher acoustic intensities formed in a confined system [19]. Production of cavitation potentially plays an important role in root canal cleaning. The production of stable cavitation may enhance streaming and mixing in the canal [20, 21], while transient cavitation produces microjets [22] and radicals [23] upon collapse. Given this potential importance of acoustic cavitation in endodontics, there is a need for detailed information with which to optimize the operating parameters for endodontic instruments. In this work, we report computational simulation of the acoustic pressure generated by endosonic instruments with the aim of predicting the occurrence of cavitation since it will occur when the acoustic pressure exceeds a threshold value [1].

Several ultrasonic systems have been studied using computational modelling approaches such as computational fluid dynamics on the fluid flow of an ultrasonic system [24, 25] and finite element analyses to predict acoustic pressure fields [26-28]. The latter was shown to give results close to the experimental sonication systems. It was used to predict optimized conditions as it was found that slight changes in geometry of the sonicating system will significantly affect the acoustic pressure fields generated [28]. Studies on fluid dynamics for dental ultrasonic systems [29, 30] have been published although there is no clear data on the acoustic pressure fields around ultrasonically driven endosonic systems under different operating conditions.

This paper aims to provide insight into the acoustic pressures generated using a computational modelling approach. In this study, the effects of power supplied, dimensions of root canal model and the dimensions of the endosonic files were examined in order to provide information of the operating conditions for different root canal dimensions with endosonic files used in clinical practice.

## 2. Materials and Methodology

### 2.1 Endosonic Files

The dimensions of the endosonic files used in the models were based on the dimensions of a standard K-file #10, #15, #20 and #25 (Endosonor, Maillefer, Dentsply) which are 15 mm long and have diameters ( $d$ ) of 0.10, 0.15, 0.20 and 0.25 mm respectively. In clinical use, these endosonic files operate on a MiniPiezon ultrasound generator (EMS, Nyon, Switzerland) at a driving frequency of 30 kHz [17]. Figure 1 illustrates a standard K-file attached to a piezoelectric hand piece.

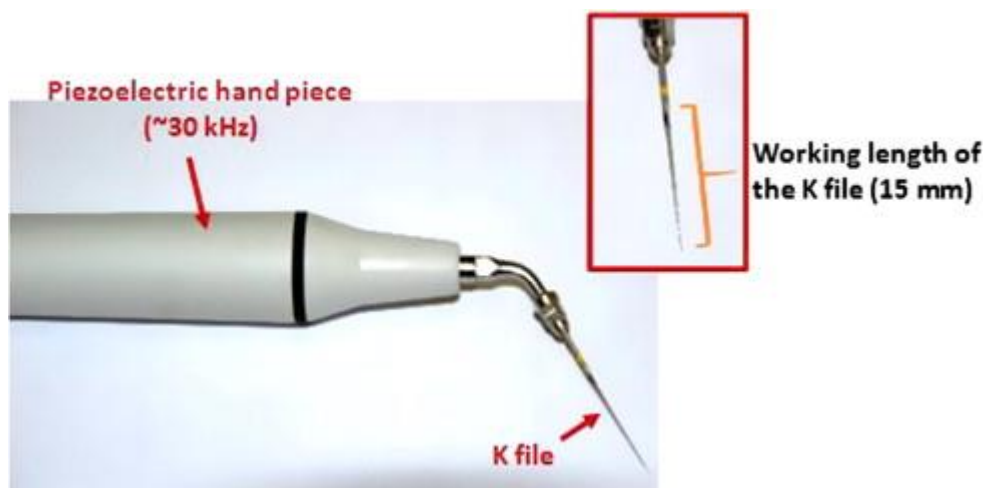


Figure 1: A standard endodontic K-file attached to a piezoelectric hand piece operating at 30 kHz. Inset: A K-file with a working length of 15 mm and diameter of 0.20 mm.

### 2.2 COMSOL Simulation Procedures

All simulations were performed using the pressure acoustics frequency domain in COMSOL Multiphysics 4.3. Simulations were performed using water as the medium in the model.

### 2.2.1 Dimensions of the root canal model

Root canals in teeth are complex structures with many channels leading from the main canal. As an initial attempt to develop a model, the root canals were simulated, as shown in Figure 2, as three dimensional cylinders with diameters ( $D$ ) of 0.8, 1.0, and 2.0 mm; and lengths ( $L$ ) of 18, 20, 22, 24 and 26 mm, corresponding to the size ranges of actual root canals [31, 32]. Models with cylinders of 5 mm and 10 mm diameters were studied to simulate operation of the endosonic files in a large working volume. The K files were represented as cylinders with dimensions described in Section 2.1, the surfaces of which acted as the acoustic emitters.

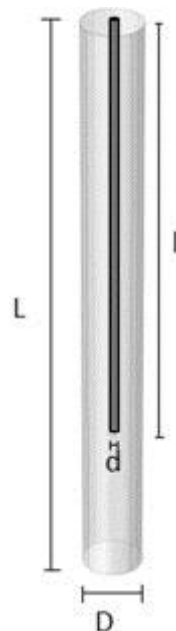


Figure 2: Representation of an endosonic file in a cylindrical root canal model. The dimensions of the endosonic file are defined by the diameter,  $d$  and length,  $l$ ; the dimensions of the root canal model are denoted by the diameter,  $D$  and length,  $L$ .



159

### 160 2.2.2 Calculation of Pressure Amplitude

161 The power dissipated into the system,  $P_{US}$ , was measured by calorimetry [33, 34] and  
162 was found to be in the range of 1 – 6 W for the systems here. The acoustic intensity,  $I$ , is  
163 obtained from Eq (1):

$$164 \quad I = \frac{P_{US}}{A} \quad (1)$$

165 where  $A = 2\pi Rl$  and is the emitting surface area of the endosonic file with  $R$  and  $l$  as the  
166 radius and length respectively. The acoustic pressure amplitude,  $p_o(r)$ , was calculated from  
167 Eq (2):

$$168 \quad I(r) = \frac{p_o^2(r)}{2\rho c} \quad (2)$$

169 Upon rearranging, gives:

$$170 \quad p_o(r) = \sqrt{\frac{2\rho c P_{US}}{A}} \quad (3)$$

171 where  $r$  is the spatial variable ( $r = [x,y,z]$ )  $\rho$  is the density of the medium and  $c$  is the sound  
172 velocity in the medium.

173

### 174 2.2.3 Acoustic Pressure Simulation

175 The acoustic pressure of the system can be obtained by solving the wave equation in  
176 COMSOL Multiphysics 4.3. Here, it is assumed that the system operates with linear wave  
177 propagation where shear stress is neglected [28]. The wave equation has the form

$$\frac{1}{\rho_o c^2} \frac{\partial^2 p}{\partial t^2} + \nabla \left( -\frac{1}{\rho_o} \nabla p \right) = 0 \quad (4)$$

where the pressure,  $P$ , is considered time harmonic.

$$P(R, t) = p(R) e^{i\omega t} \quad (5)$$

where  $\omega$  is the angular frequency. This simplifies to the Helmholtz equation

$$\nabla \left( -\frac{1}{\rho_o} \nabla p \right) - \frac{\omega^2}{\rho_o c^2} p = 0 \quad (6)$$

The Helmholtz equation can be solved by a variety of numerical methods [26, 28, 35] when suitable boundary conditions are applied. The accuracy of the simulation is subjected to a natural rule of adjustment where

$$\kappa \cdot h = \text{constant} \quad (7)$$

with the wave number,  $\kappa = \omega/c$ . The stepsize,  $h$ , of the numerical solution method [36] is adjustment by changing the number of elements in the finite element model or by using small meshes to increase the resolution to decrease the pollution effect in the model [37]. The mesh generation used for this work was a predefined tetrahedral mesh with improved resolution at the curvatures, totalling up to 60981 elements and 90170 number of degree of freedoms, for a system of 1 mm diameter and 20 mm length. The simulated results were validated by gradually increasing the mesh numbers until negligible effect was obtained from the solution generated. Figure 3 illustrates the generated mesh with extra-fine grids generated along the endosonic files.

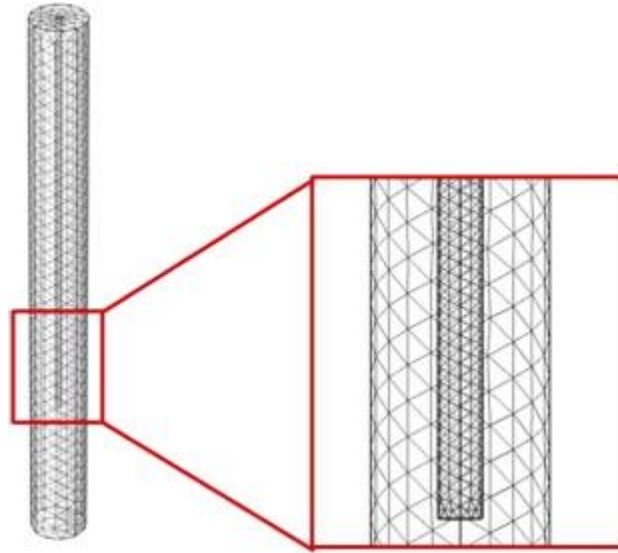


Figure 3: Tetrahedral mesh generated around the endosonic file and the root canal model for finite element analysis for COMSOL modelling. This sums up to a total of 104956 elements for this particular model.

#### 2.2.4 Boundary Conditions

The boundary conditions of the model used were:

- (i) The edges of the endosonic file as hard wall boundaries, assuming  $p = p_o$  and  $\frac{\partial p}{\partial n} = 0$ , where  $p$  is the acoustic pressure and  $n$  is the normal vector to the boundary surface.
- (ii) The air-water interface as a soft boundary where  $p = 0$ , indicating total reflection of ultrasound.
- (iii) The walls of the root canal model as material with the acoustic properties of dentin, having an acoustic impedance ( $Z$ ) of 7.8 MRayl [38].

#### 2.2.1 Validation of Simulation

A series of proof – of – principle simulations were performed as described elsewhere [39] by simulating results on a 20 kHz ultrasonic horn system which were compared with experimental results [27, 28].

### 3. Results and Discussion

#### 3.1 Effects of Output Power

Figure 4 illustrates the simulated acoustic pressure fields generated around a vibrating file with dimensions of 0.25 mm ( $d$ )  $\times$  15 mm ( $l$ ) contained in a cylinder of 1 mm ( $D$ )  $\times$  20 mm ( $L$ ) at an output power of 6W. Regions of high acoustic pressure are illustrated in red and low acoustic pressures are in blue. The areas of highest acoustic pressure are around the mid-length of the file, suggesting this to be where the highest tendency for cavitation to occur.

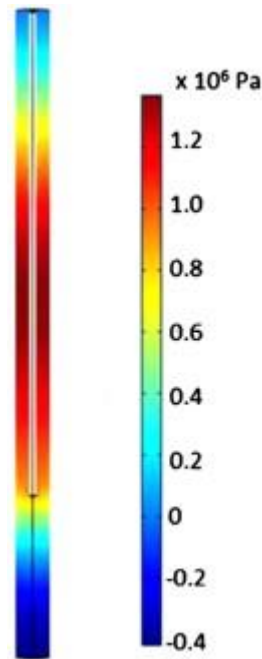


Figure 4: Acoustic pressure fields generated along the  $y$ - $z$  field for an endosonic file (0.25 mm,  $d \times 15$  mm,  $l$ ) in a root canal model (1 mm,  $D \times 20$  mm,  $L$ ) ranging from -0.4 to 1.3 MPa for an endosonic file with power output of 6W.

Table 1 collates reported values of the threshold acoustic pressure needed to generate cavitation in water. Generally, the acoustic pressure threshold ranges from 0.1 MPa for 100 % air saturated water to 20 MPa for 0.1 % of air saturation in a reactor [40]. It was reported that cavitation threshold lies in the range of approximately 1.4 MPa in a polymethyl methacrylate (PMMA) microchannel of 3 mm diameter [41]. A similar magnitude of the cavitation threshold has been reported in human tissue in lithotripsy [42]. The cavitation threshold pressures depend strongly on differences in operating frequency and the types of reactors used. In general, an acoustic pressure of approximately 1.4 – 1.5 MPa is required to generate cavitation in a confined space, though care must be taken that this can vary with different operating dimensions, frequency and intensity.

Figure 5 shows the variation of predicted maximum acoustic pressure fields that could be obtained within the root canal model environment as a function of output power. The values range from 0.5 MPa at 1 W to 1.3 MPa at 6 W. These values are comparable with the cavitation threshold so it can be deduced that it is possible that transient cavitation could occur when high powers are supplied to endosonic files.

Table 1: Collated cavitation threshold pressures and acoustic reaction conditions of different systems.

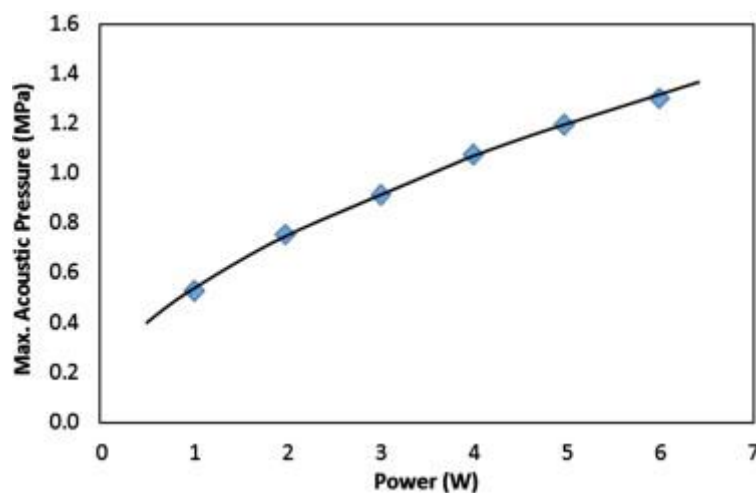


Figure 5: Maximum acoustic pressure generated within the root canal model at various power outputs for an endosonic file (0.25 mm,  $d \times 15$  mm,  $l$ ) in a root canal model (1 mm,  $D \times 20$  mm,  $L$ ).

### 3.2 Effects of the Size of the Root Canal Model

The anatomy of real root canals is very complex and consists of many branched fine channels [31]. The bottom of the root canal is usually unreachable in endodontic practice [45]. Production of acoustic cavitation aids in the streaming [14, 15] of the irrigant inside an infected root canal and in its cleaning [5, 8]. Therefore, in order to evaluate the potential for cavitation to enhance root canal treatment, it is important to look at the change of the maximum acoustic pressure generated when the dimensions of the root canal vary. Figure 6 illustrates the isobaric lines of acoustic pressure generated in a vessel of 10 mm diameter. These isobaric lines signifies a certain region of similar acoustic pressure generated around the model. The simulations show that there is an area of maximum acoustic pressure generated (in red) at the end of the endosonic file with the second highest acoustic pressure achieved around the middle of the file (in orange). These results can be compared with previous experimental measurements of the oscillations of the endosonic files of similar dimensions [17] which showed maximum oscillation amplitudes in these regions, showing the strong correlation between oscillation amplitude and the production of acoustic pressure in an ultrasonic system. It can also be seen some areas of high acoustic pressure are produced at the bottom of the vessel. This may be due to the reflection and constructive interference of the acoustic field. Nevertheless, based on the acoustic cavitation threshold pressure prediction of 1.4 MPa, it can be seen that the simulated pressures are lower so that it is unlikely that cavitation would be observed when the endosonic file is operated in a large volume of water.

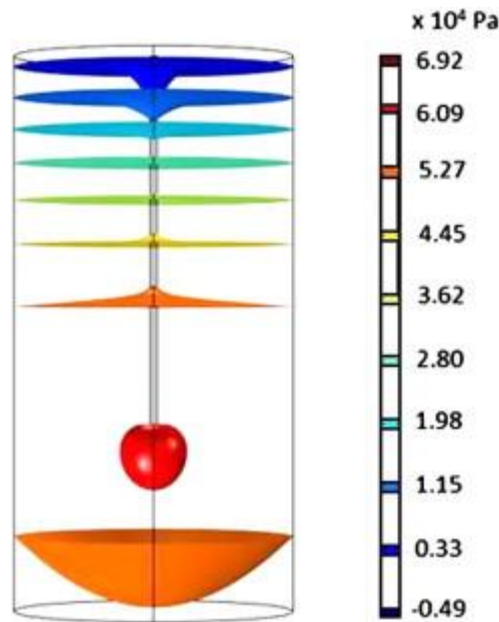


Figure 6: Isobaric lines showing the acoustic pressure areas generated around a root canal model by an endosonic file (0.25 mm,  $d \times 15$  mm,  $l$ ) operating at 6 W in a root canal model (10 mm,  $D \times 20$  mm,  $L$ ).

Decreasing the size of the container in which the file oscillates, simulating operation in a narrower root canal, results in significant increases in the in maximum acoustic pressure generated in the system. Figure 7 shows the effects of acoustic pressure with different root canal model diameters. It shows that the pressures change little in large containers but increase by up to ten-fold when the channel diameter becomes comparable with the file diameter. The results agree with those from the recent work of Macedo *et al.* [19], who have observed a significant rise in the emission of sonochemiluminescence (SCL) produced when the working volume was decreased – which serves as an indication of cavitation produced in high acoustic pressure regions. The intensity of ultrasound attenuates with distance [46] so decrease in acoustic pressure in a large working volume is to be expected. This is also supported by a study who had reported that cavitation occurs at higher intensities when it is in a confined space [41].

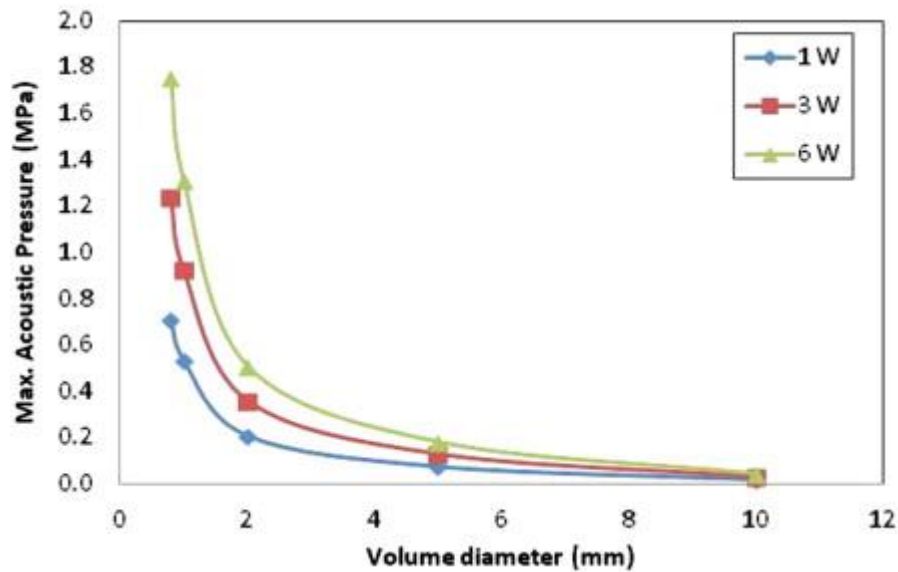


Figure 7: Maximum acoustic pressure generated in different root canal diameters by an endosonic file (0.25 mm,  $d \times 15$  mm,  $l$ ) at powers 1W, 3W and 6W respectively.

One observation of the report on the SCL produced with an endosonic file in a human-sized root canal models is that it forms uniform distribution of SCL in the entire root canal [19]. This phenomena is different from what was previously reported on SCL production in a bulk solution, where localized distribution were observed on certain areas along the endosonic files [6, 33]. Again, this can be explained by the acoustic pressure distribution in different volumes, as illustrated in Figure 8. From Figure 8(a), it can be seen that a large proportion of the area possess high enough acoustic pressure ( $> 1.4$  MPa) to generate cavitation in a small volume but not in a larger container as in Figure 8(b). This suggests that if cavitation were to occur in a large volume of water, it will be localized to areas close to the ultrasonic source.



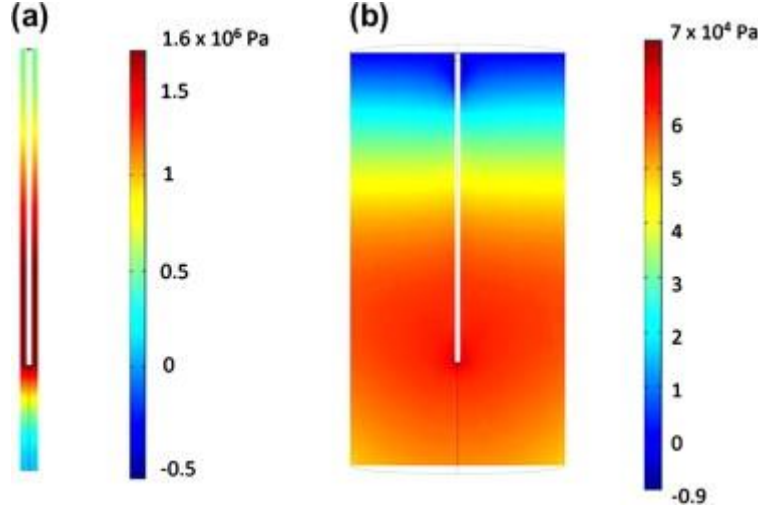


Figure 8: Acoustic pressure fields generated by an endosonic file (0.25 mm,  $d \times 15$  mm,  $l$ ) at 6W, in (a) 0.8 mm diameter, 20 mm length root canal model; and (b) 10 mm diameter, 20 mm length root canal model.

It was reported that the acoustic pressure,  $p_o$ , formed from an ultrasound horn with radius  $r$  decreases with distance from the source,  $x$ , according to

$$p_o \approx \sin \frac{k}{2} \left( \sqrt{x^2 + r^2} - x \right) \quad (8)$$

Equation 8 indicates a 95 % reduction in  $p_o$ , at a distance twice the horn radius [28]. However, the situation will be different for dental instruments since, whereas an ultrasonic horn vibrates in an up – down motion [47] while ultrasonically driven dental instruments vibrate in an irregular circular motion [48]. This complicates the calculation on the decrease in intensity in terms of distance from the ultrasonic source. Equation (9) can be used to obtain a quantitative measurement to account for the percentage of attenuation (or transmission loss,  $TL$ ) [49]

$$TL = 10 \log_{10} \left[ \frac{P_{US,in}}{P_{US,out}} \right] \quad (9)$$

where  $P_{US,in}$  and  $P_{US,out}$  can be obtained by integrating

$$P_{US} = \int \frac{p_o^2}{2\rho c} dA \quad (10)$$

where  $p_o$  is the acoustic pressure,  $\rho$  is the density of the medium,  $c$  is the speed of sound in the medium and  $A$  is the area of the emitting surface.  $P_{US,in}$  is the ultrasonic power inlet, obtained based on the ultrasonic source – in this case is the endosonic file; while  $P_{US,out}$  is the power outlet, calculated based on the acoustic pressure at the walls of the root canal model [49]. Figure 9 shows the transmission loss when the endosonic files were operated in root canal models of different diameters and demonstrates that it is lower when the file is operated in a confined space. A significant increase in transmission loss can be seen from 7 dB to 10 dB when the diameter increases from 0.8 to 2 mm and further increases occur at wider diameters, albeit to a smaller extent. The work demonstrates that, in a large working volume, the acoustic pressure generated in the surrounding fluid undergoes higher attenuation as it travels away from the ultrasonic source, generating a much lower total acoustic pressure in the liquid.

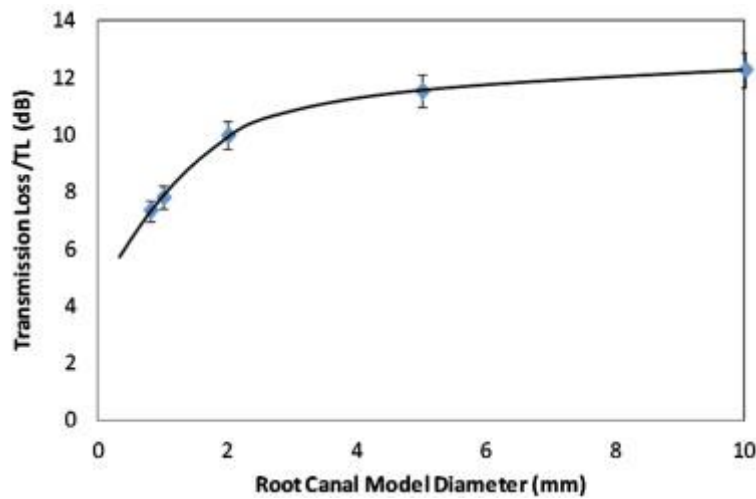


Figure 9: Effects of canal diameter on transmission loss generated by an endosonic file (0.25 mm,  $d \times 15$  mm,  $l$ ) in a root canal model of 20 mm length.

Due to the acoustic impedance mismatch between water and the walls of the root canal model which are assumed to have the properties of dentin, when a sound wave from the endosonic file passes through water and hits the walls of the root canal model, it is partially reflected, causing a general increase in acoustic pressure fields in a confined area. The reflective ( $R_c$ ) and transmission ( $T_c$ ) coefficients of a longitudinal wave are given by

$$R_c = \left( \frac{Z_2 - Z_1}{Z_2 + Z_1} \right)^2 \quad (11)$$

$$T_c = \frac{4Z_2Z_1}{(Z_2 + Z_1)^2} \quad (12)$$

where  $Z_1$  and  $Z_2$  are the acoustic impedances of the material where sound wave propagates from and travels into respectively. For this work,  $R_c = 0.46$  and  $T_c = 0.54$ , suggesting that almost half of the sound energy will be reflected back into the water. Table 2 collates  $R_c$  values for different experiments conducted in a confined space. Higher impedance mismatch between water and the walls of the system results in higher reflective coefficient. Hence, it can be deduced that the cavitation threshold pressure for an endosonic file in a root canal could be lower than 1.4 MPa, seeing that almost half of the acoustic wave will be reflected back into the system.

Table 2: Collated results of the acoustic impedance, cavitation threshold pressure and reflective coefficient of different systems conducted in a confined space.

The effect of different root canal lengths on the maximum acoustic pressure generated was examined with the results in Figure 10. There is a small decrease in the maximum acoustic pressure generated in the liquid as the root canal model gets longer. This is not significant in narrow canals of 0.8 mm diameter where a standard deviation of 4 % was found. However, the differences become more apparent in wider channels of 1.0 and 2.0 mm

diameter, where decrement of 7 – 10 % in acoustic pressure was found when the diameter of the endosonic file increases from 18 to 22 mm, followed by a slight increment of 5 – 7 % for endosonic files of 22 – 26 mm length. The differences in acoustic pressure may be contributed by the reflection in acoustic pressure formed from the bottom of the vessel (Figure 6).

Figure 11 illustrates the acoustic pressures generated along the length of the walls of the root canal model. The dashed lines give an indication of the cavitation threshold 1.4 MPa [40] both at the positive and negative sides of the acoustic pressure graph. Though cavitation does not occur at the positive acoustic cycle, however, note must be taken that this simulation is a time harmonic simulation. The nodal points of the sound source travelling along the endosonic file switches sides along with the acoustic cycle. A small shift in the acoustic pressure profile can be seen when the length of the root canal model increases, but this did not affect the areas of possible acoustic cavitation activity, which fell in the range of approximately 8 to 17 mm along the length of the root canal model. This also suggests that cavitation might be possible approximately 1 – 2 mm below the end of the endosonic file.

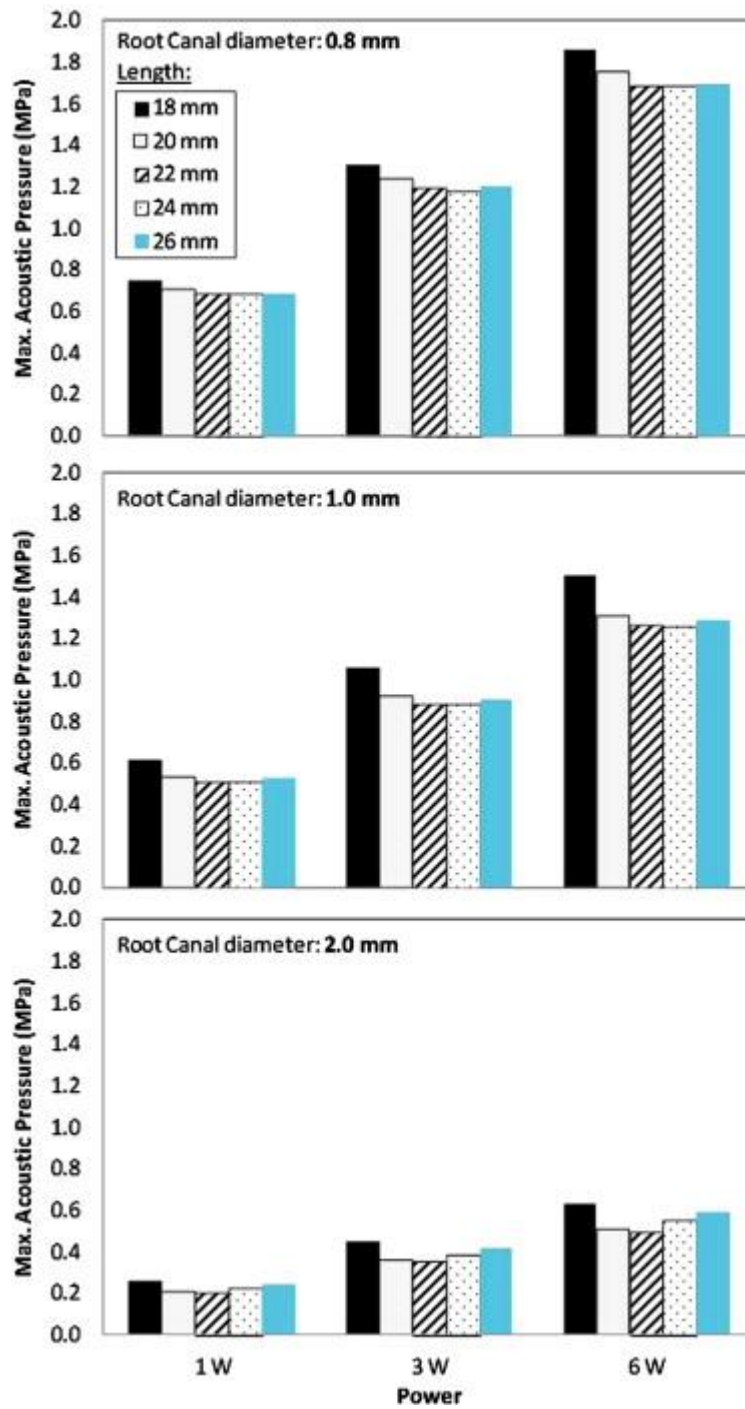


Figure 10: Maximum acoustic pressure generated by an endosonic file (0.25 mm,  $d \times 15$  mm,  $l$ ) in a root canal model of different dimensions.

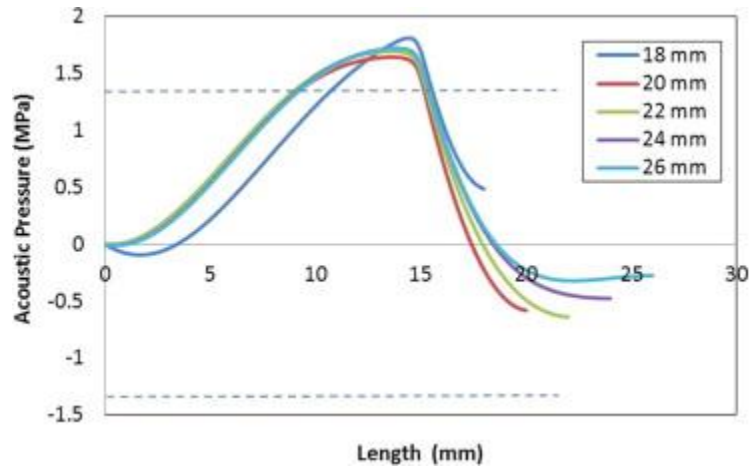


Figure 11: Effects of channel length on acoustic pressure generated using an endosonic file (0.25 mm,  $d \times 15$  mm,  $l$ ) at 6W in a channel with width 0.8 mm.

Similar calculations of the transmission loss were performed based on Eq. (9) and (10) for different lengths of the root canal model. They showed that changing the length from 18 to 26 mm does not have much effect much on the attenuation (Figure 12). This is correlated to the direction of travel of the wave since an endosonic file vibrates in the  $x$  and  $z$  directions but not the  $y$  direction [48] hence a greater effect of different diameters rather than the length of the root canal might be expected.

### 3.3 Effects of the Shape and Size of the Endosonic Files

In practice, a real endosonic file is not a perfect cylindrical-shape but is more of a flat-tipped cone with larger diameter at the top and narrower tip at the bottom. This study examined the significant differences in acoustic pressure generated by a cylindrical and a cone-shaped endosonic file under the same operating conditions.

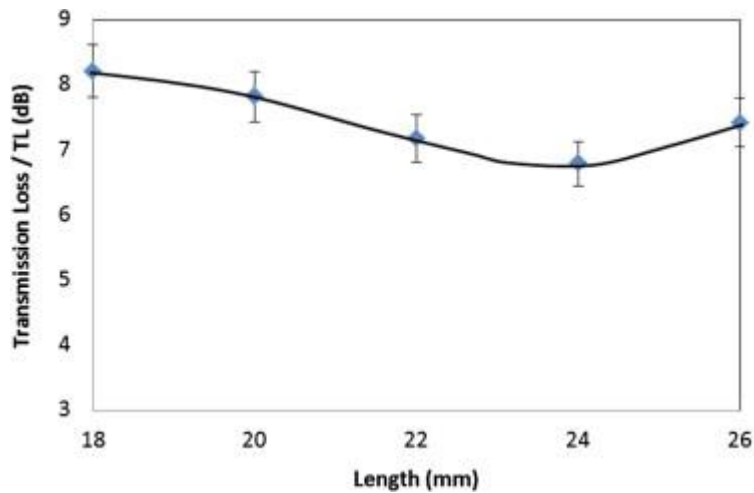


Figure 12: Effect on canal length on transmission loss generated by an endosonic file of 0.25 mm diameter and 15 mm length in a root canal model of 0.8 mm diameter.

Figure 13 shows the maximum acoustic pressures are not significantly different for this change of shape for smaller file diameters but does become more apparent at larger diameters. There is also a trend of higher acoustic pressure generated with increasing file diameters. This further supports previous studies [6, 8, 33] on the lack of SCL production in thinner dental files due to insufficient surface area to generate the necessary high acoustic pressure fields in the system.

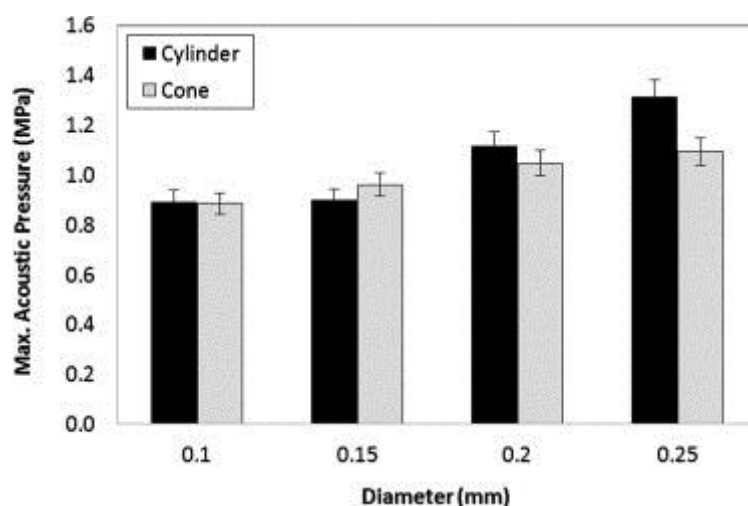


Figure 13: Maximum acoustic pressure generated by 15 mm length cylindrical and cone shaped endosonic files with different diameters in a root canal model of 1 mm diameter and 20 mm length.

#### 4. Conclusions

The acoustic pressure fields generated by endosonic files with varying dimensions have been calculated using the COMSOL simulation package. It was found that maximum acoustic pressures of 1.3 MPa, in excess of the cavitation threshold, can be achieved in a confined system of 1 mm ( $D$ )  $\times$  20 mm ( $L$ ) at an output power of 6 W, comparable with conditions used in clinical practice. This indicates the possibility of the generation of cavitation at high power settings in a root canal model.

Investigation on the effects of root canal model diameter and length showed that higher acoustic pressures were achieved in root canal models of smaller dimensions due to lower transmission losses in the system. Changing the root canal length did not significantly affect the maximum acoustic pressure generated, but it was observed that the highest acoustic pressures were generally generated at around 8 to 17 mm into the length of the root canal model. The difference between cone and cylindrical shaped endosonic files did not have an effect the acoustic pressure for narrow files but had a significant difference on file with 0.25 mm diameter.

This study has provided a good insight on acoustic pressure generation for dental endosonic instruments in a condition mimicking the root canal profile in a human's tooth. The results obtained showed close correlation to those reported in the literature and serve as a good methodology for future optimization of ultrasonically driven dental instruments.

#### References

- [1] F.R. Young, Cavitation, London : Imperial College Press, London, 1999.
- [2] S.A. Elder, Cavitation Microstreaming, J. Acoust. Soc. Am., 31 (1959) 54-64.
- [3] K.S. Suslick, M.M. Fang, T. Hyeon, M.M. Mdleleni, Applications of Sonochemistry to Materials Synthesis, in: L.A. Crum, T.J. Mason, J. Reisse, K.S. Suslick (Eds.) Sonochemistry and Sonoluminescence, Kluwer Publishers, Dordrecht, Netherlands, 1999, pp. 291-320.



- [4] A.D. Walmsley, S.C. Lea, G. Landini, A.J. Moses, Advances in power driven pocket/root instrumentation, *Journal of Clinical Periodontology*, 35 (2008) 22-28.
- [5] S.C. Lea, G.J. Price, A.D. Walmsley, A study to determine whether cavitation occurs around dental ultrasonic scaling instruments, *Ultrasonics Sonochemistry*, 12 (2005) 233-236.
- [6] B. Felver, D.C. King, S.C. Lea, G.J. Price, A.D. Walmsley, Cavitation occurrence around ultrasonic dental scalers, *Ultrasonics Sonochemistry*, 16 (2009) 692-697.
- [7] M. Sanz, W. Teughels, A.o.t.E.W.o.P. on behalf of group, Innovations in non-surgical periodontal therapy: Consensus Report of the Sixth European Workshop on Periodontology, *Journal of Clinical Periodontology*, 35 (2008) 3-7.
- [8] T.J. Tiong, G.J. Price, Ultrasound promoted reaction of Rhodamine B with sodium hypochlorite using sonochemical and dental ultrasonic instruments, *Ultrasonics Sonochemistry*, 19 (2012) 358-364.
- [9] B.A.A. Scheven, R.M. Shelton, P.R. Cooper, A.D. Walmsley, A.J. Smith, Therapeutic ultrasound for dental tissue repair, *Medical Hypotheses*, 73 (2009) 591-593.
- [10] S.J. Lee, M.K. Wu, P.R. Wesselink, The efficacy of ultrasonic irrigation to remove artificially placed dentine debris from different-sized simulated plastic root canals, *International Endodontic Journal*, 37 (2004) 607-612.
- [11] L.W.M. Van Der Sluis, M. Versluis, M.K. Wu, P.R. Wesselink, Passive ultrasonic irrigation of the root canal: a review of the literature, *International Endodontic Journal*, 40 (2007) 415-426.
- [12] D.R. Violich, N.P. Chandler, The smear layer in endodontics – a review, *International Endodontic Journal*, 43 (2010) 2-15.
- [13] M. Ahmad, T.R. Pitt Ford, L.A. Crum, A.J. Walton, Ultrasonic Debridement of Root Canals: Acoustic Cavitation and Its Relevance\*, *International Endodontic Journal*, 42 (2009) 391-398.
- [14] A.D. Walmsley, W.R.E. Laird, A.R. Williams, Dental plaque removal by cavitation activity during ultrasonic scaling, *Journal of Clinical Periodontology*, 15 (1988) 539-543.
- [15] P.J. Lumley, P.S.K. Lucarotti, F.J.T. Burke, Ten - year outcome of root fillings in the General Dental Services in England and Wales, *International Endodontic Journal*, 41 (2008) 577-585.
- [16] A.D. Walmsley, A.R. Williams, Effects of constraint on the oscillatory pattern of endosonic files, *Journal of Endodontics*, 15 (1989) 189-194.
- [17] S.C. Lea, A.D. Walmsley, P.J. Lumley, Analyzing Endosonic Root Canal File Oscillations: An In Vitro Evaluation, *Journal of Endodontics*, 36 (2010) 880-883.
- [18] B. Verhaagen, S.C. Lea, G.J. De Bruin, L.W.M. Van Der Sluis, A.D. Walmsley, M. Versluis, Oscillation characteristics of endodontic files: numerical model and its validation, *Ultrasonics, Ferroelectrics and Frequency Control, IEEE Transactions on*, 59 (2012) 2448-2459.
- [19] R.G. Macedo, B. Verhaagen, D. Fernandez Rivas, J.G.E. Gardeniers, L.W.M. van der Sluis, P.R. Wesselink, M. Versluis, Sonochemical and high-speed optical characterization of cavitation generated by an ultrasonically oscillating dental file in root canal models, *Ultrasonics Sonochemistry*, 21 (2014) 324-335.
- [20] N.M. Maurits, G.E. Loots, A.E.P. Veldman, The influence of vessel wall elasticity and peripheral resistance on the carotid artery flow wave form: A CFD model compared to in vivo ultrasound measurements, *Journal of Biomechanics*, 40 (2007) 427-436.
- [21] F. Parvizian, M. Rahimi, S.M. Hosseini, S.S. Madaeni, A.A. Alsairafi, The effect of high frequency ultrasound on diffusion boundary layer resistance in ion-exchange membrane transport, *Desalination*, 286 (2012) 155-165.
- [22] V. Raman, A. Abbas, S.C. Joshi, Mapping Local Cavitation Events in High Intensity Ultrasound Fields, in: *Proceedings of the COMSOL Users Conference 2006, Bangalore, 2006*.
- [23] V. Sáez, A. Frías-Ferrer, J. Iniesta, J. González-García, A. Aldaz, E. Riera, Characterization of a 20 kHz sonoreactor. Part I: analysis of mechanical effects by classical and numerical methods, *Ultrasonics Sonochemistry*, 12 (2005) 59-65.
- [24] J. Klíma, A. Frias-Ferrer, J. González-García, J. Ludvík, V. Sáez, J. Iniesta, Optimisation of 20 kHz sonoreactor geometry on the basis of numerical simulation of local ultrasonic intensity and qualitative comparison with experimental results, *Ultrasonics Sonochemistry*, 14 (2007) 19-28.
- [25] C. Boutsioukis, B. Verhaagen, M. Versluis, E. Kastrinakis, L.W. van der Sluis, Irrigant flow in the root canal: experimental validation of an unsteady Computational Fluid Dynamics model using high-speed imaging, *Int Endod J*, 43 (2010) 393-403.

- [26] C. Boutsoukis, B. Verhaagen, M. Versluis, E. Kastrinakis, P.R. Wesselink, L.W. van der Sluis, Evaluation of irrigant flow in the root canal using different needle types by an unsteady computational fluid dynamics model, *J Endod*, 36 (2010) 875-879.
- [27] R.H. Liu, J. Yang, M.Z. Pindera, M. Athavale, P. Grodzinski, Bubble-induced acoustic micromixing, *Lab on a Chip*, 2 (2002) 151-157.
- [28] P. Marmottant, M. Versluis, N. de Jong, S. Hilgenfeldt, D. Lohse, High-speed imaging of an ultrasound-driven bubble in contact with a wall: "Narcissus" effect and resolved acoustic streaming, *Experimental Methods and their Applications to Fluid Flow*, 41 (2006) 147-153.
- [29] L.A. Crum, Surface Oscillations and Jet Development in Pulsating Bubbles, *Journal de Physique*, 41 (1979) 285-288.
- [30] K. Makino, M.M. Mossoba, P. Riesz, Chemical effects of ultrasound on aqueous solutions. Formation of hydroxyl radicals and hydrogen atoms, *The Journal of Physical Chemistry*, 87 (1983) 1369-1377.
- [31] P. Carrotte, Endodontics: Part 4 Morphology of the root canal system, *British Dental Journal*, 197 (2004) 379.
- [32] C. Sathorn, J.E. Palamara, D. Palamara, H.H. Messer, Effect of root canal size and external root surface morphology on fracture susceptibility and pattern: a finite element analysis, *J Endod*, 31 (2005) 288-292.
- [33] T.J. Tjong, D.C. King, S.C. Lea, A.D. Walmsley, G.J. Price, Correlation of vibrometry and cleaning effects in ultrasonic dental instruments, in: 20th International Congress on Acoustics 2010, ICA 2010 - Incorporating Proceedings of the 2010 Annual Conference of the Australian Acoustical Society., Sydney, Australia., 2010, pp. 604-609.
- [34] D.C. King, Sonochemical analysis of the output of ultrasonic dental descalers, in: Department of Chemistry, University of Bath, Bath, United Kingdom, 2011, pp. 146-148.
- [35] F. Ihlenburg, Finite element analysis of acoustic scattering, New York : Springer, New York, 1998.
- [36] F. Ihlenburg, I. Babuška, Finite element solution of the Helmholtz equation with high wave number Part I: The h-version of the FEM, *Computers & Mathematics with Applications*, 30 (1995) 9-37.
- [37] I. Babuška, F. Ihlenburg, T. Strouboulis, S.K. Gangaraj, A posteriori error estimation for finite element solutions of Helmholtz' equation—Part II: estimation of the pollution error, *International Journal for Numerical Methods in Engineering*, 40 (1997) 3883-3900.
- [38] R.S. Singh, M.O. Culjat, W.S. Grundfest, E.R. Brown, Tissue mimicking materials for dental ultrasound, *J. Acoust. Soc. Am.*, 123 (2008) EL39-EL44.
- [39] T.J. Tjong, Sonochemical and ultrasonic output analyses on dental endosonic instruments, PhD Thesis in: Department of Chemistry, University of Bath, Bath, United Kingdom., 2012, pp. 176-237.
- [40] W.J. Galloway, An Experimental Study of Acoustically Induced Cavitation in Liquids, *The Journal of the Acoustical Society of America*, 26 (1954) 849-857.
- [41] Y. Iida, K. Yasui, T. Tuziuti, M. Sivakumar, Y. Endo, Ultrasonic cavitation in microspace, *Chemical Communications*, (2004) 2280-2281.
- [42] A.J. Coleman, T. Kodama, M.J. Choi, T. Adams, J.E. Saunders, The cavitation threshold of human tissue exposed to 0.2-MHz pulsed ultrasound: preliminary measurements based on a study of clinical lithotripsy, *Ultrasound Med Biol*, 21 (1995) 405-417.
- [43] S. Leicht, K. Raum, Acoustic impedance changes in cartilage and subchondral bone due to primary arthrosis, *Ultrasonics*, 48 (2008) 613-620.
- [44] K. Zell, J.I. Sperl, M.W. Vogel, R. Niessner, C. Haisch, Acoustical properties of selected tissue phantom materials for ultrasound imaging, *Physics in Medicine and Biology*, 52 (2007) N475-N484.
- [45] M.K. Wu, H. Shemesh, P.R. Wesselink, Limitations of previously published systematic reviews evaluating the outcome of endodontic treatment, *International Endodontic Journal*, 42 (2009) 656-666.
- [46] T.G. Leighton, The acoustic bubble, London : Academic Press, San Diego, United States of America, 1997.
- [47] L. Soo Il, H. Sang Hyuk, Nonlinear vibration analysis of ultrasonic horn model for flip-chip bonding, in: Control, Automation and Systems, 2007. ICCAS '07. International Conference on, 2007, pp. 2804-2807.

- 533 [48] S.C. Lea, G. Landini, Reconstruction of dental ultrasonic scaler 3D vibration patterns from  
534 phase-related data, *Medical Engineering and Physics*, 32 (2010) 673-677.  
535 [49] COMSOL, COMSOL Multiphysics User's Guide, (2011)